Available online at www.sciencedirect.com
SCIENCE DIRECT
Carbon 44 (2006) 629–637
CARBON
www.elsevier.com/locate/carbon

Catalytic growth of macroscopic carbon nanofiber bodies with high bulk density and high mechanical strength

M.K. van der Lee, A.J. van Dillen, J.W. Geus, K.P. de Jong, J.H. Bitter *

Department of Inorganic Chemistry and Catalysis, Debye Institute, Utrecht University, P.O. Box 80 083, 3508 TB Utrecht, Netherlands

Received 29 July 2005; accepted 28 September 2005
Available online 8 November 2005

Abstract

Carbon nanofibers (CNF) are non-microporous graphitic materials with a high surface area (100–200 m^2/g), high purity and tunable surface chemistry. Therefore the material has a high potential for use as catalyst support. However, in some instances it is claimed that the low density and low mechanical strength of the macroscopic particles hamper their application. In this study we show that the bulk density and mechanical strength of CNF bodies can be tuned to values comparable to that of commercial fluid-bed and fixed-bed catalysts. The fibers were prepared by the chemical decomposition of CO/H_2 over Ni/SiO_2 catalysts. The resulting fibers bodies (1.2 mm) were replicates of the Ni/SiO_2 bodies (0.5 mm) from which they were grown. The bulk density of CNF bodies crucially depended on the metal loading in the growth catalyst. Over 5 wt% Ni/SiO_2 low density bodies (0.4 g/ml) are obtained while 20 wt% Ni/SiO_2 leads to bulk densities up to 0.9 g/ml with a bulk crushing strength of 1.2 MPa. The 20 wt% catalysts grow fibers with diameters of ~22 nm, which grow irregularly in space, resulting in a higher entanglement and a concomitant higher density and strength as compared to the thinner fibers (~12 nm) grown from 5 wt% Ni/SiO_2.

Keywords: Carbon nanofibers; Catalytic grown carbon; Catalyst support; Texture; Density

1. Introduction

Carbon fibers (CNF) are graphite-like materials, which hold great potential as catalyst support [1–21]. However, at a number of occasions it is claimed that these materials are obtained as "fluffy materials" i.e., having a low bulk density [2,22–24] and a low mechanical strength [2]. This would not allow the economic use in a reactor since the mass of catalyst per reactor volume is too low. In addition, due to the mechanical weakness of those materials, application in large fixed-bed reactors, fluidized-bed or slurry-phase reactors is not viable. Therefore synthesis routes to CNF bodies with high bulk densities and high strength are much desired.

Different methods to prepare CNF are described in literature, a.o., arc discharge [25–28], decomposition of organometallic compounds [29–31] or chemical vapor deposition [32–35] of carbon containing gases over metal catalysts, i.e., catalytic growth [36–41]. The latter option is preferred for large-scale production of CNF [42,43]. Essential in the growth of CNF is the decomposition of the carbon source on the surface of the metal particles. The thus formed carbon atoms migrate through/over the metal to assemble into CNF [1,2,44,45]. CNF growth critically depends on a number of factors such as temperature, nature of the catalyst and source of carbon [1,2,20,39,46–55].

It is claimed that the CNF can form three-dimensional networks of interwoven fibers resulting in bodies of micrometer size which are replicates of the original shape of the catalyst particles from which they were grown [2,56–59]. Typically the formed CNF bodies increase with a factor 3 in diameter compared to the size of the catalyst particles [56]. Thus when a fine powder is used as starting material the resulting CNF bodies also consist of small

* Corresponding author. Fax: +31 30 251 1027.
E-mail address: J.H.Bitter@chem.uu.nl (J.H. Bitter).

0008-6223/$ - see front matter © 2005 Elsevier Ltd. All rights reserved.
doi:10.1016/j.carbon.2005.09.031

bodies. This can explain why some authors obtain CNF as powder while others obtain macroscopically shaped CNF bodies [56–59].

Literature revealed that when CNF are grown with a low rate irregularly shaped fibers can be formed which strongly entangle with each other [1,2,44]. This potentially can lead to highly dense materials, which can be mechanically strong as well. The final density of the material depends crucially on the way in which the CNF are grown. For example Hoogenraad [2] obtained CNF with a bulk density of 0.35 g/ml grown from 20 wt% Ni/Al_2O_3 using methane as the carbon source while Reshetenko [23] obtained a bulk density of 0.76 g/ml over a highly loaded 90 wt% Ni/Al_2O_3 catalyst. Besides the different nickel loading, Reshetenko used a vibro-fluid-bed reactor and pure methane as carbon source at 773 K while Hoogenraad used a fixed-bed reactor with diluted methane gasflows at 823 K.

In the current contribution we investigate the role of the growth catalysts, in particular the metal loading, on the bulk density and strength of the prepared CNF bodies.

We chose Ni/SiO_2 as the growth catalyst because SiO_2 has significant advantages over the use of Al_2O_3 when pure CNF are desired. SiO_2 is conveniently removed by a treatment of the prepared materials by a solution of KOH [44]. In case of Al_2O_3 acid extraction is needed while full removal of the support is cumbersome [45]. For the silica-based catalyst in a separate step the exposed growth catalyst (Ni) is removed by a treatment in concentrated HCl [16,44].

General agreement exists on the fact that the diameter of the CNF is always similar to that of the metal particle from which it is grown [2,56–59]. In earlier studies it is found that the size of Ni particles in the CNF can be significantly larger than those in the fresh growth catalysts [1,2,40,56]. Clearly a sintering step is involved during the CNF growth. This sintering only occurred during CNF growth since in inert or hydrogen atmospheres at temperatures even higher than the CNF growth temperature sintering did not occur [60,61]. Since sintering appears to be an important issue in CNF preparation we choose to use for our study two Ni/SiO_2 catalysts having similar Ni particles sizes but different metal loadings (5 and 20 wt%) i.e., different sintering rates can be expected. The influence of the metal loading will be shown to have a crucial influence on the properties (yield and density) of the CNF bodies.

2. Experimental

2.1. Preparation of growth catalyst

Five or 20 wt% Ni/SiO_2 catalysts were prepared by deposition precipitation as described by Van Dillen et al. [63] using 10.0 g silica (Degussa, Aerosil 200, powder), nickel nitrate (Acros) and urea (Acros). After washing, filtration and drying at 393 K the catalyst precursor was calcined in static air at 873 K.

2.2. CNF preparation

Prior to the carbon nanofiber growth 0.4 g of the nickel–silica growth catalyst, sieve fraction 425–850 μm, was placed in a quartz upflow fixed-bed reactor (internal diameter 25 mm) and reduced in situ for 2 h in a flow of a mixture of H_2 (80 ml/min) and N_2 (320 ml/min) at 1 bar and at 973 K (heating rate 5 K/min). Next, the fibers were grown at 823 K in a mixture of CO (120 ml/min), H_2 (42 ml/min) and N_2 (238 ml/min) for 1, 2, 4, 6 or 20 h. The product (including the growth catalyst) was refluxed for 2 h in 200 ml of an aqueous 1 M KOH solution to remove the silica support. Next, after filtering and thoroughly washing with de-ionised water, the fibers were refluxed in concentrated HCl, to remove exposed nickel followed by washing and drying.

2.3. Characterization

XRD patterns were recorded at room temperature with an Enraf Nonius PDF 120 powder diffractometer system equipped with a position-sensitive detector with a 2θ range of 120° using Co $K\alpha_1$ ($\lambda = 1.78897$ Å) radiation. Average particle sizes were calculated using the Debye–Scherrer equation.

Nitrogen physisorption was carried out at 77 K using a Micromeritics Tristar 3000 V 6.01. Prior to the physisorption measurement the samples were dried in a He flow at 573 K. For the analysis of the average pore diameter the BJH method was applied to the desorption isotherm.

Scanning electron microscopy (SEM) was carried out using a Philips XL30 FEG apparatus. The samples were placed on a carbon coated sample holder. In case of the CNF bodies, both intact and cleaved CNF bodies were investigated. The intact bodies were used to scan the outside of the skeins. The cleaved bodies were analyzed both on the outside as well as on the cleaved facet of the body.

TEM samples were prepared by suspending the fibers after grinding in ethanol under ultrasonic vibration. Some drops of the thus produced suspension were brought onto a holey carbon film on a copper grid. The grid was transferred to a FEG-Technai-20 TEM apparatus operated at 200 keV.

2.4. Bulk density of carbon nanofiber bodies

The bulk density of grown carbon nanofibers was determined by measuring the mass of a fixed volume. A fixed volume, i.e., a glass cylinder, was filled without vibration, with the CNF bodies in accordance to the American Standard Test Methods (ASTM D1895-96 B).

2.5. Bulk crushing strength

About 17 ml of carbon nanofibers bodies with a body size larger than 425 μm were packed in a steel container. Pressures from 0.2 to 3.1 MPa were applied on the stacked

CNF bodies via a steel dye. With increasing pressure the CNF bodies break and as a result fines (bodies < 425 μm) were formed. The cumulatively weight of the fines was determined as function of the applied pressure. The bulk crushing strength (BCS) is defined as the pressure at which cumulatively 0.5 wt% fines are formed.

3. Results

Some of the physico-chemical properties of the Ni/SiO_2 growth catalysts have been compiled in Table 1. Although the Ni-particle size of Ni-5 and Ni-20 are similar, the density of particles is much higher for Ni-20, see Fig. 1. The Ni particle size distribution of Ni-20 seems to be somewhat broadened as well. Low magnification SEM images have been collected to report the bodies shapes and sizes. Fig. 2A and B show the SEM images of the original Ni/SiO_2 growth catalyst Ni-5 and Ni-20. Fig. 2C–F gives a macroscopic overview of the CNF bodies formed after 1 and 20 h over Ni-5 and Ni-20 resulting in CNF-5-*x* or CNF-20-*x* with *x* representing the growth time in hours. It can be noted that irrespective of the applied growth conditions the CNF skeins have similar shapes as the original growth catalysts. However, after 1 h the bodies are smaller than the original Ni/SiO_2 bodies while after 20 h they are larger.

On a mesoscopic scale significant differences can be observed among the different samples. In Fig. 3 SEM micrographs of CNF-5-20 and CNF-20-20 are shown. The top part of Fig. 3A and B shows the outer surface of the CNF bodies while the lower part (C and D) displays the inside. The diameter distributions of the fibers on the surface the inside of the bodies after 1 and 20 h of growth obtained from TEM images have been compiled in Fig. 4. After 1 h of growth clearly from Ni-5 smaller diameter (8–16 nm) CNF were grown compared to those from Ni-20 (16–30 nm). All CNF used in this study are of the fishbone type as shown by a representative high resolution TEM micrograph (Fig. 5).

The fiber diameter distribution as determined by TEM of CNF-5-1 and CNF-20-1 (Fig. 4) both shift to larger diameters with longer growth times. SEM images show that for CNF-5–20 well defined individual CNF can be observed (Fig. 3), while for CNF-20-20 a densely packed structure is formed inside the CNF bodies. Some textural and structural properties of the prepared samples are given in Table 2. In line with the decrease in BET surface area the observed diameter of the CNF increases. From the BET surface area and assuming a carbon density of 2.25 g/cm^3 and closed solid fibers a diameter for the fibers can be calculated (Table 2; d_{calc}). Clearly the calculated fiber diameter based on BET is smaller than those obtained from SEM although the trends in diameter variation with time are similar. Recently we have reported that CNF may contain internal cylindrical pores of about 5–10 nm which explains the higher diameter values from TEM compared to those from the specific surface areas [64].

Fig. 6 shows the yield of CNF per gram nickel as function of the growth time and as function of the growth catalyst. Ni-5 shows a linear increase in CNF yield as function of time. On the other hand, Ni-20 initially grows CNF with a higher rate but the rate declines with time.

The bulk density of the CNF bodies as function of growth catalyst and growth time is displayed in Fig. 7. For CNF-5 an initial decrease in the bulk density was observed after which it remained constant around 0.4 g/ml. For CNF-20 an initial sharp increase of the bulk density was found from 0.5 after 1 h CNF growth to 0.8 g/ml after 6 h of growth. Finally after 20 h of growth skeins with a bulk density of 0.9 g/ml were obtained.

Table 1
Some physico-chemical properties of Ni/SiO_2 growth catalysts reduced at 973 K for 2 h in H_2

	Nominal Ni loading (wt%)	Ni d_p (nm)		S_{BET} (m^2/g)	PV (ml/g)
		XRD	TEM		
Ni-5	5	4	4	181	1.26
Ni-20	20	5	5	217	0.85

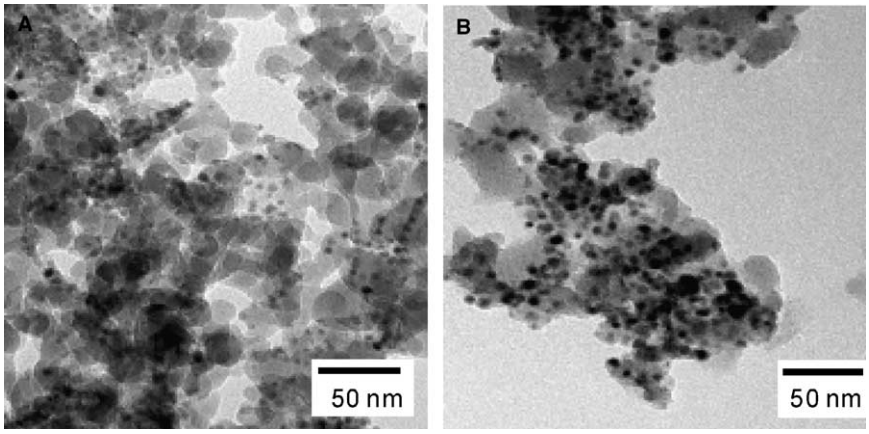

Fig. 1. TEM images of growth catalysts after reduction at 973 K: (A) 5 wt% Ni/SiO_2 and (B) 20 wt% Ni/SiO_2.

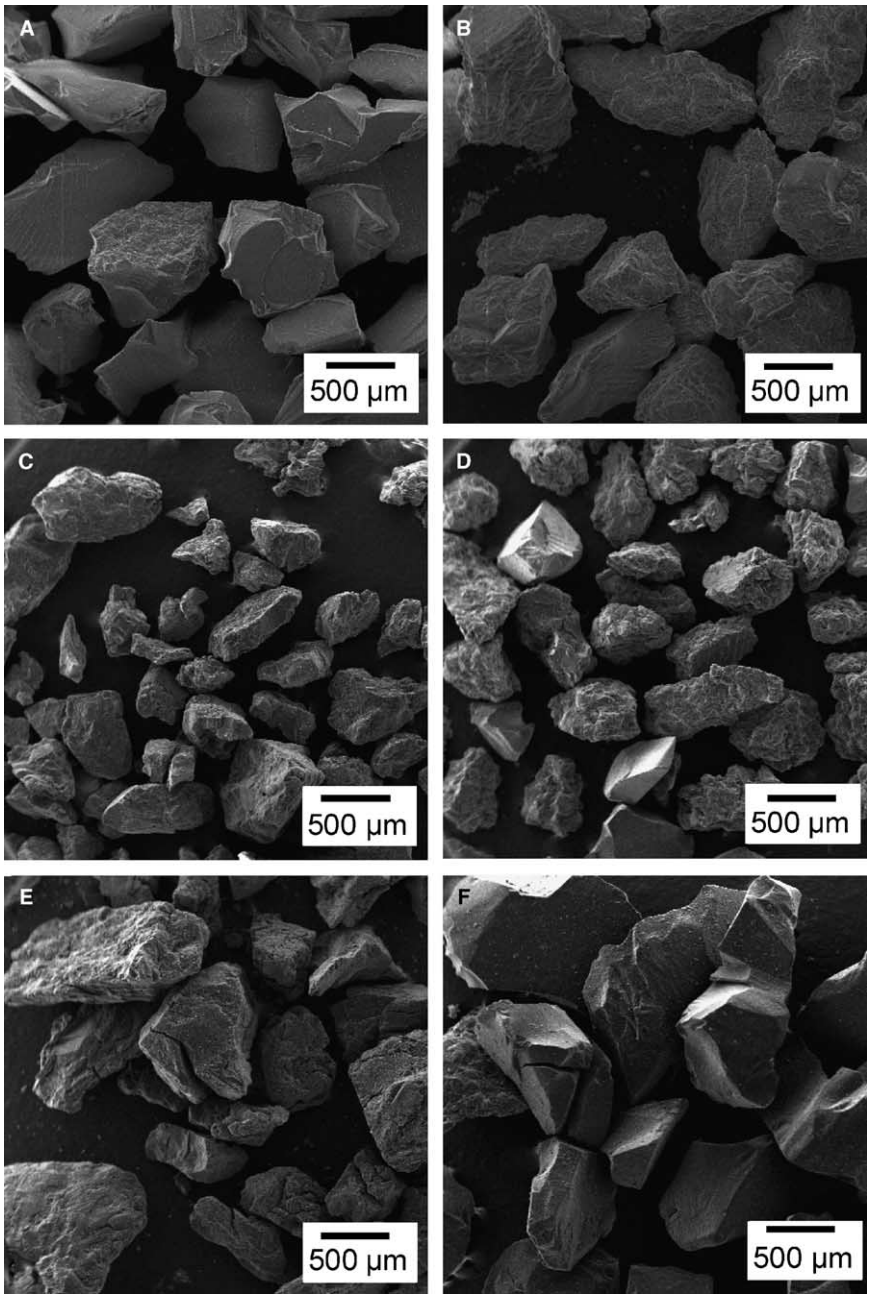

Fig. 2. Low magnification SEM images of growth catalyst after reduction 973 K and grown CNF bodies: (A) 5 wt% Ni/SiO_2; (B) 20 wt% Ni/SiO_2; (C) CNF bodies CNF-5-1; (D) CNF bodies CNF-20-1; (E) CNF bodies CNF-5-20; (F) CNF bodies CNF-20-20.

As shown in Fig. 6 the mass of CNF produced increases with time. On the other hand the bulk density increases for CNF prepared with Ni-20 but remains constant with time over Ni-5 (Fig. 7). Therefore it is interesting to know what the influence of growth time and nickel catalyst loading is on the size of the CNF bodies prepared. Fig. 8 shows the average body size as function of time. For CNF prepared over both catalysts an initial decrease in the body size is observed while after 1 h of growth the size increases again. The latter being with a higher rate over Ni-5 compared to Ni-20.

The high bulk density of the Ni-20-20 material (0.9 g/ml) is comparable to or above that of commercial catalysts [66]. In addition the bulk crushing strength of the CNF-20-20 bodies was found to be 1.25 MPa (Fig. 9) which make them suitable for fixed-bed applications [56]. The CNF bodies already disintegrate due to weak forces and their bulk crushing strength was estimated to be <0.5 MPa.

4. Discussion

Figs. 1 and 2 give an overview of the used Ni/SiO_2 catalyst. The physico-chemical properties of these materials are summarized in Table 1. Close inspection and analysis of the micrographs of the CNF (Fig. 3) reveals that all

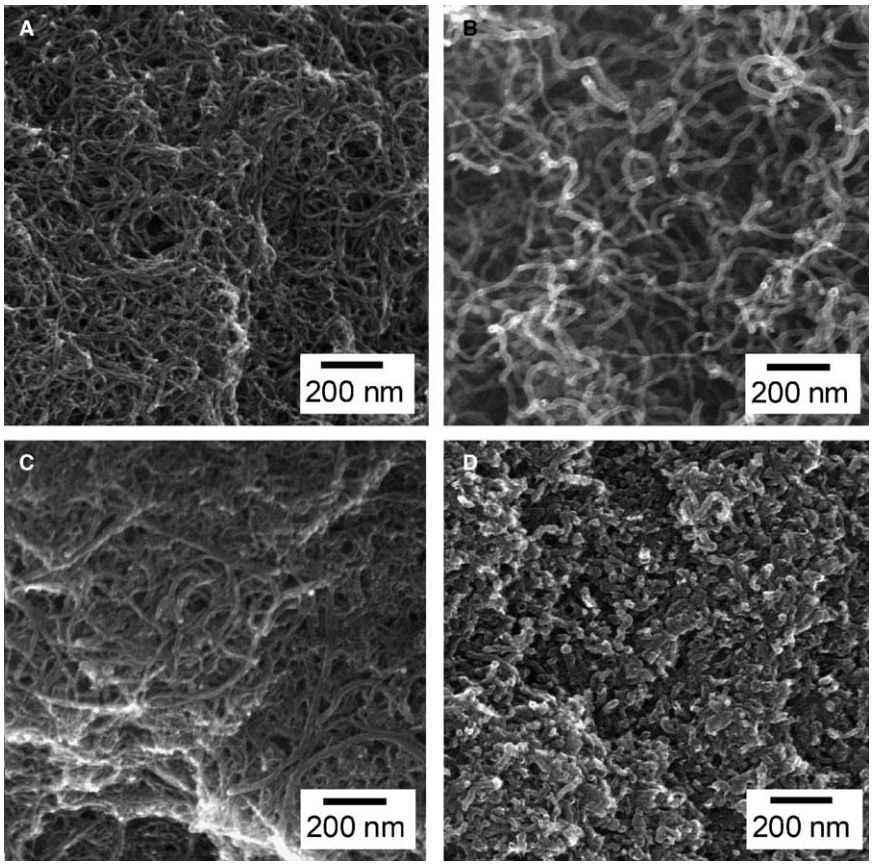

Fig. 3. High magnification SEM images of carbon nanofibers grown for 20 h using Ni-5 or Ni-20 growth catalyst: (A) outside CNF-5-20; (B) outside of CNF-20-20; (C) inside CNF-5-20; (D) inside of the CNF-20-20.

fibers in the bodies, irrespective of the growth conditions, have a larger diameter (8–40 nm, Fig. 4) than the Ni particles from which they were grown (~5 nm; Table 1 and Fig. 1). At many occasions it has been shown that the diameter of the grown CNF closely matches that of the Ni particles at the top of the fibers [2,32,44,56,64,65] from which the fibers were grown. Thus it must be concluded that in some stage the initial small Ni particles (~5 nm) have sintered to larger particles (8–40 nm).

Most likely, sintering occurs prior to the start of the CNF growth. This is also supported by the fact that small metal particles (<5 nm) retard the formation of graphene sheets since their surface is strongly curved [2,44]. In earlier studies [44,62] we showed that the Ni particles in Ni/SiO_2 do not sinter significantly in H_2 atmosphere. Therefore the carbon containing gas is a pre-requisite for sintering. Since in Ni-20 the concentration of Ni particles is higher compared to that in Ni-5 it can be expected that (a) the sintering is more significant over Ni-20 due to the closer proximity of the Ni particles and (b) the CNF growth rate is higher over Ni-20 due to the higher amount of active metal which is in line with what is observed (Fig. 6). This is in agreement with the thicker fibers, which are formed over Ni-20 (Fig. 4). From Ni-5 with an initial particle size of 4 nm (Table 1) CNF with an average diameter of 12 nm were grown (Fig. 4) while from Ni-20 with an initial Ni particle size of 5 nm (Table 1) CNF with an average diameter of 22 nm were grown (Fig. 4). From this is can be estimated that roughly 6 times more Ni is involved in the growth of a single fiber from Ni-20 as compared to Ni-5 which is not too remote from the difference in metal loading in both catalysts.

The thicker fibers e.g., CNF-20-20, grow in bodies with a higher bulk density as compared to the thin fibers which grow in less dense bodies (Fig. 7). This can be explained by the different growth mechanism of large and small diameter fibers. Large diameter fibers grow via the so-called rice-shell mechanism resulting in irregular shaped fibers [1,2,44]. Here the growth of CNF is not a continuous process but is periodical [2,56,67]. The metal particle is converted to metal carbide while a significant fraction of the metal surface is encapsulated by carbon. When a certain carbide concentration has been reached the encapsulating shell burst and the Ni whole particle becomes available again for growth. The driving force for the excretion of the fiber is a lowering of the density of the metal/carbide phase via demixing of the metal and the carbide. In this ''start-stop-start-stop'' mechanism every start of growth can be in a different direction resulting in curved fibers which strongly entangle. The thin CNF grow via a continuous carbon dissolution–excretion model. In the latter mechanism the rate of carbide formation in the metal

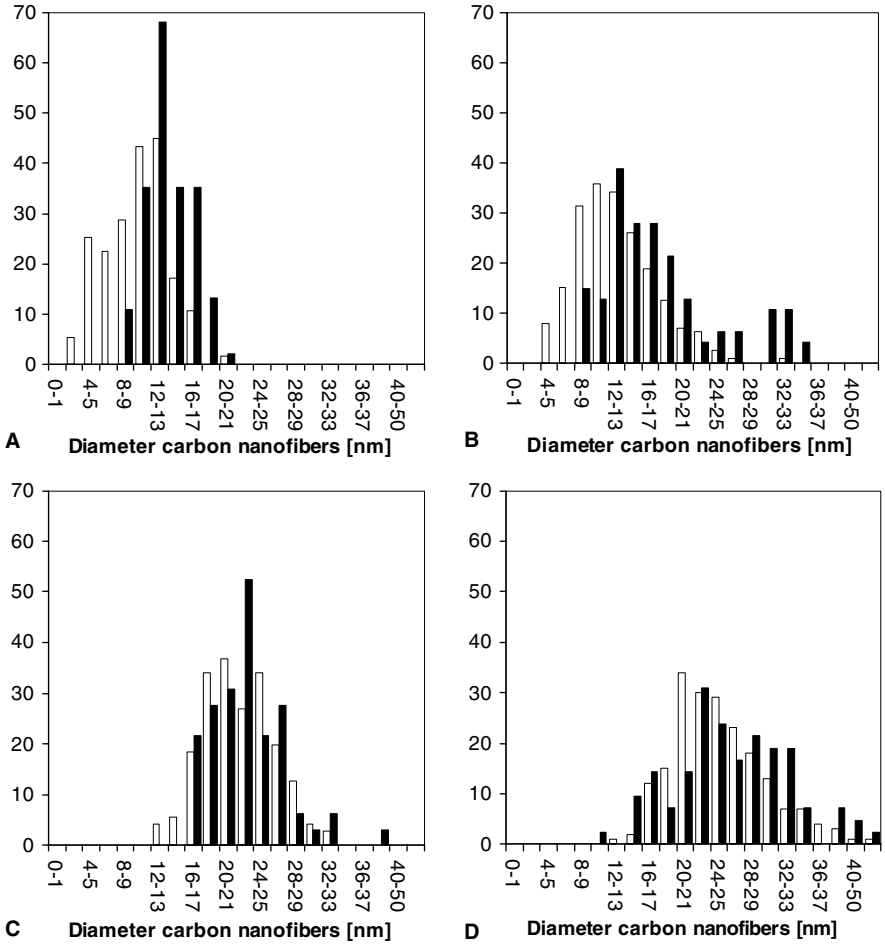

Fig. 4. Carbon nanofiber diameter distribution inside (black bars) and at outside (open bars) of the CNF body: (A) CNF-5-1; (B) CNF-5-20; (C) CNF-20-1; (D) CNF-20-20.

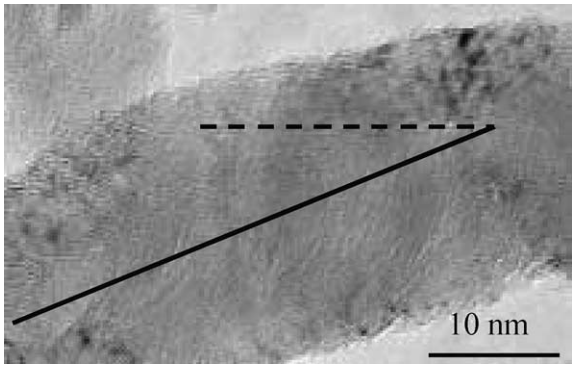

Fig. 5. HRTEM of the fishbone fibers. Dashed line: direction of graphene sheets; solid line: fiber axis.

particle is balanced by the formation of the carbon fibers, which results in the continuous growth rate of CNF, which are more straight (Fig. 3) [2,67].

After having established the nature of the CNF growth processes on a mesoscopic scale it turns out that the growth conditions also have an influence on the size of the formed bodies (Figs. 2 and 8) i.e., on a macroscopic scale. Fig. 8 shows clearly that irrespective of the growth catalyst first a decrease in body size is observed as function of the amount of CNF formed. This is the result of fragmentation of the initial Ni/SiO_2 bodies into smaller bodies. Because the bulk density of CNF-5 does not increase with time (Fig. 7) while the yield of CNF does (Fig. 6) it must be concluded that this material grows in a voluminous way in which the increase in CNF yield results in a continuous expansion of the bodies resulting in a constant bulk density. This does not hold for Ni-20, since after the initial decrease of the CNF body size it increases, however, with a lower rate as compared to Ni-5 as inferred from Fig. 6 by the lower slope between 4–20 g C/g Ni. Thus the newly formed CNF in CNF-20 grow in the empty spaces inside the bodies resulting in a lower expansion rate of the bodies, thus, resulting in a higher bulk density as compared to CNF-5. The higher bulk density of CNF-20-*x* compared to that of CNF-5-*x* is in line with the mesoscopic growth mechanism discussed above. Since thicker fibers, i.e., those in CNF-20-*x* grown in an irregular way, are bent resulting in a high entanglement resulting in a high bulk density. The straight thinner fibers in CNF-5-*x* on the other hand grow

Table 2
Some physico-chemical properties of the CNF bodies

	Growth catalyst	Growth time (h)	S_{BET} (m^2/g)	PV (ml/g)	d_{obs} [nm] (TEM)	d_{calc} [nm] (BET)
CNF-5-1	Ni-5	1	232	0.69	10	8
CNF-5-4	Ni-5	4	167	0.85		11
CNF-5-6	Ni-5	6	208	0.84		9
CNF-5-20	Ni-5	20	197	0.73	12	9
CNF-20-1	Ni-20	1	165	0.68	20	11
CNF-20-4	Ni-20	4	160	0.32		11
CNF-20-6	Ni-20	6	151	0.25		12
CNF-20-20	Ni-20	20	130	0.19	24	14

Silica from growth catalysts was removed by refluxing CNF bodies in 1 M KOH for 2 h. BET and pore volume are based on nitrogen physisorption.

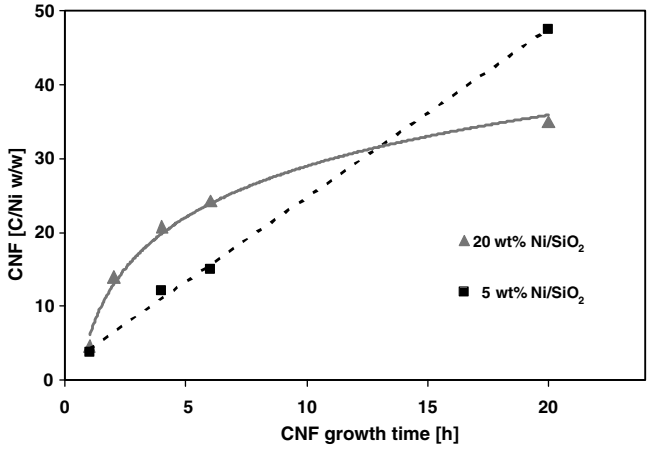

Fig. 6. CNF yield (gram carbon per gram nickel) as function of time and metal loading in the growth catalyst.

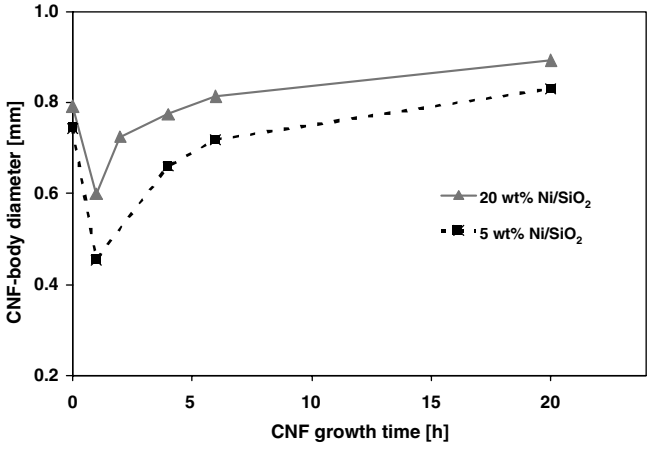

Fig. 8. CNF-body size as function of growth time. At 0 h the average diameter of original Ni/SiO_2 particles are shown for Ni-5 and Ni-20 catalysts.

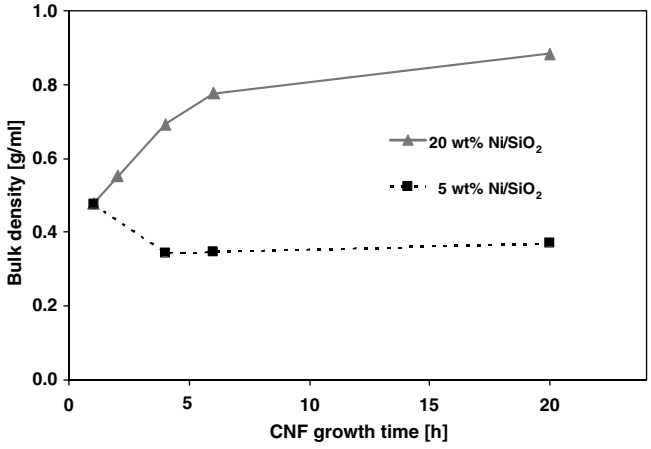

Fig. 7. Bulk density of CNF as function of the metal loading in the growth catalyst and growth time.

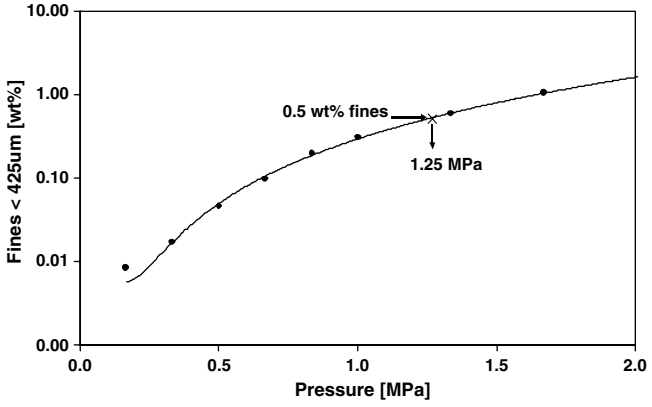

Fig. 9. Cumulative amount of fines measured as function of pressure during bulk crushing strength analysis of the Ni-20-20 CNF bodies.

faster and do not entangle very well resulting in a low bulk density.

Since we were never able to detect large patches of SiO_2 by TEM/EDX, before SiO_2 removal, it is concluded that the SiO_2 is completely fragmentized during the growth process. This is schematically shown in Fig. 10. The initially formed CNF break up the weak Ni/SiO_2 body in smaller fragments. Next the fibers on the inside start to grow in all directions thus continuously expanding the much stronger CNF body resulting in replicates of fragments of the original SiO_2 body [56–59]. The properties of the CNF-20-20 bodies are such that they are suitable for commercial application at least in fixed-bed reactors [66]. Different

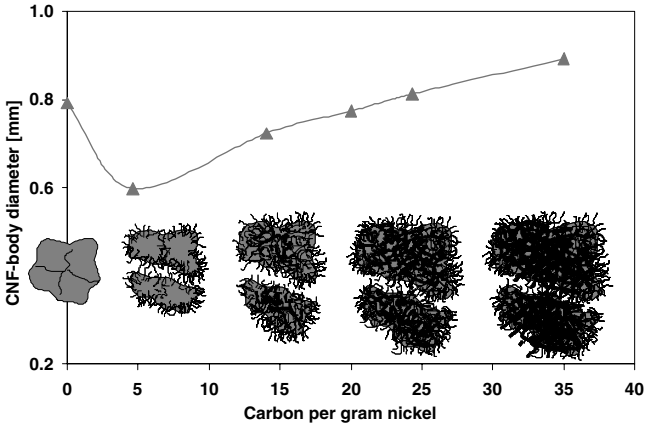

Fig. 10. Schematic representation of macroscopic bodies consisting of dense CNF growth from left to right: Ni/SiO_2 body with cracks—growing CNF fragmentize the body—start of large diameter growth CNF in interior—further expansion of CNF body.

ways of metal deposition on these materials are put forward in literature, e.g. [13,16,20,21,66,68,69] resulting in catalyst which can be among the most active one for e.g., cinnamaldehyde hydrogenation [16].

5. Conclusions

The diameter of carbon nanofibers (CNF) formed over Ni/SiO_2 was dependent on the metal loading in the growth catalyst. When starting with identical nickel particle sizes (5 nm) a highly loaded Ni/SiO_2 catalyst (20 wt%) resulted in fibers with a average diameter of ~22 nm. These bodies had a high bulk density of 0.9 g/ml and high mechanical strength making these materials suitable for applications in a fixed-bed reactor. Lower loaded Ni/SiO_2 (5 wt%) led to straight ~12 nm fibers throughout the CNF body. The formation of straight fibers relates to the lower density of the formed CNF bodies, which are replicas of the Ni/SiO_2 growth catalyst. The thicker fibers formed over 20 wt% Ni/SiO_2 were more entangled due to their bent shapes which resulted in high bulk density and high mechanical strength of the CNF bodies.

Acknowledgement

The authors acknowledge STW for financial support (grant UPC 5487).

References

[1] De Jong KP, Geus JW. Carbon nanofibers: catalytic synthesis and applications. Catal Rev—Sci Eng 2000;42:481–510.
[2] Hoogenraad MS. Ph.D. thesis, Utrecht University, Utrecht, The Netherlands, 1995.
[3] Serp P, Corrias M, Kalck P. Carbon nanotubes and nanofibers in catalysis. Appl Catal A Gen 2003;253:337–58.
[4] Hoogenraad MS, Onwezen MF, Van Dillen AJ, Geus JW. Supported catalysts based on carbon fibrils. Stud Surf Sci Catal 1996; 101: 1331–9.
[5] Geus JW, Hoogenraad MS, Van Dillen AJ. In: Iglesia E, Lednor PW, Nagaki DA, Thompson LT, editors. Synthesis and properties of advanced catalytic materials. Pittsburgh: Materials Res. Soc.; 1995. p. 87–98.
[6] Hoogenraad MS, Van Leeuwarden RAGMM, Van Breda Vriesman GJB, Broersma A, Van Dillen AJ, Geus JW. In: Poncelet G, editor. Preparation of catalysts VI. Amsterdam: Elsevier; 1995. p. 263–71.
[7] Mojet BL, Hoogenraad MS, Van Dillen AJ, Geus JW, Koningsberger DC. Coordination of palladium on carbon fibrils as determined with XAFS spectroscopy. J Chem Soc Faraday Trans 1997;93:4371–5.
[8] Rodriguez NM, Kim MS, Baker RTK. Carbon nanofibers: a unique catalyst support medium. J Phys Chem 1994;98:13108–11.
[9] Chambers A, Nemes T, Rodriguez NM, Baker RTK. Catalytic behavior of graphite nanofiber supported nickel particles. 1. Comparison with other support media. J Phys Chem B 1998; 102:2251–8.
[10] Park C, Baker RTK. Catalytic behavior of graphite nanofiber supported nickel particles. 2. The influence of the nanofiber structure. J Phys Chem B 1998;102:5168–77.
[11] Park C, Baker RTK. Catalytic behavior of graphite nanofiber supported nickel particles. 3. The effect of chemical blocking on the performance of the system. J Phys Chem B 1999;103:2453–9.
[12] Salman F, Park C, Baker RTK. Hydrogenation of crotonaldehyde over graphite nanofiber supported nickel. Catal Today 1999;53:385–94.
[13] Pham-Huu C, Keller N, Charbonniere LJ, Ziessel R, Ledoux MJ. Carbon nanofiber supported palladium catalyst for liquid-phase reactions. An active and selective catalyst for hydrogenation of CC bonds. Chem Commun 2000;19:1871–2.
[14] Planeix JM, Coustel N, Coq B, Brotons V, Kumbhar PS, Dutartre R, et al. Application of carbon nanotubes as supports in heterogeneous catalysis. J Am Chem Soc 1994;116:7935–6.
[15] Ang LM, Andy Hor TS, Xu GQ, Tung CH, Zhao S, Wang JLS. Electroless plating of metals onto carbon nanotubes activated by a single-step activation method. Chem Mater 1999;11:2115–8.
[16] Toebes ML, Zhang Y, Hajek J, Nijhuis TA, Bitter JH, Van Dillen AJ, et al. Support effects in the hydrogenation of cinnamaldehyde over carbon nanofiber-supported platinum catalysts: characterization and catalysis. J Catal 2004;226:215–25.
[17] Jarrah N, Van Ommen JG, Lefferts L. Development of monolith with a carbon-nanofiber-washcoat as a structured catalyst support in liquid phase. Catal Today 2003;79:29–33.
[18] Toebes ML, Prinsloo FF, Bitter JH, Van Dillen AJ, De Jong KP. Influence of oxygen-containing surface groups on the activity and selectivity of carbon nanofiber-supported ruthenium catalysts in the hydrogenation of cinnamaldehyde. J Catal 2003;214:78–87.
[19] Pham-Huu C, Keller N, Ehret G, Charbonniere LJ, Ziessel R, Ledoux MJ. Carbon nanofiber supported palladium catalyst for liquid-phase reactions—an active and selective catalyst for hydrogenation of cinnamaldehyde into hydrocinnamaldehyde. J Mol Catal A—Chem 2001;170:155–63.
[20] Ros TG, Keller DE, Van Dillen AJ, Geus JW, Koningsberger DC. Preparation and activity of small rhodium metal particles on fishbone carbon nanofibres. J Catal 2002;211:85–102.
[21] Reshetenko TV, Avdeeva LB, Ismagilov ZR, Chuvilin AL. Catalytic filamentous carbon as supports for nickel catalysts. Carbon 2004;42:143–8.
[22] Qiu J, Li Y, Wang Y. Novel fluffy carbon balls obtained from coal which consist of short curly carbon fibres. Carbon 2004;42:2359–62.
[23] Reshetenko TV, Avdeeva LB, Ismagilov ZR, Pushkarev VV, Cherepanova SV, Chuvilin AL, et al. Catalytic filamentous carbon—structural and textural properties. Carbon 2003;41:1605–15.
[24] Wang Y, Wei F, Gu G, Yu H. Agglomerated carbon nanotubes and its mass production in a fluidized-bed reactor. Physica B 2002;323:327–9.
[25] Li L, Li F, Liu C, Cheng HM. Synthesis and characterization of double-walled carbon nanotubes from multi-walled carbon nanotubes by hydrogen-arc discharge. Carbon 2005;43:623–9.

[26] Huang H, Kajiura H, Murakami Y, Ata M. Metal sulfide catalyzed growth of carbon nanofibers and nanotubes. Carbon 2003;41:615–8.
[27] Seraphin S, Wang S, Zhou D, Jiao J. Strings of spherical carbon clusters grown in a catalytic arc discharge. Chem Phys Lett 1994;228:506–12.
[28] Kajiura H, Huang H, Tsutsui S, Murakami Y, Miyakoshi M. High-purity fibrous carbon deposit on the anode surface in hydrogen DC arc-discharge. Carbon 2002;40:2423–8.
[29] Tibbetts GG. Vapor-grown carbon fibers: status and prospects. Carbon 1989;27:745–7.
[30] Schnitzler MC, Oliveira MM, Ugarte D, Zarbin AJG. One-step route to iron oxide-filled carbon nanotubes and bucky-onions based on the pyrolysis of organometallic precursors. Chem Phys Lett 2003;381:541–8.
[31] Satishkumar BC, Govindaraj A, Sen R, Rao CNR. Single-walled nanotubes by the pyrolysis of acetylene–organometallic mixtures. Chem Phys Lett 1998;293:47–52.
[32] Zheng GB, Kouda K, Sano H, Uchiyama Y, Shi YF, Quan HJ. A model for the structure and growth of carbon nanofibers synthesized by the CVD method using nickel as a catalyst. Carbon 2004;42:635–40.
[33] Yoon YJ, Baik HK. Catalytic growth mechanism of carbon nanofibers through chemical vapor deposition. Diam Relat Mater 2001;10:1214–7.
[34] Serp P, Madroñero A, Figueiredo JL. Production of vapour-grown carbon fibres: influence of the catalyst precursor and operating conditions. Fuel 1999;78:837–44.
[35] Ci L, Li Y, Wei B, Liang J, Xu C, Wu D. Preparation of carbon nanofibers by the floating catalyst method. Carbon 2000;38:1933–7.
[36] Trimm DL. The formation and removal of coke from nickel catalyst. Catal Rev—Sci Eng 1977;16:155–89.
[37] Rostrup-Nielsen JR, Trimm DL. Mechanisms of carbon formation on nickel-containing catalysts. J Catal 1977;48:155–65.
[38] Bartholomew CH. Carbon deposition in steam reforming and methanation. Catal Rev—Sci Eng 1982;24:67–111.
[39] Figueiredo JL. Filamentous carbon. Erdol Kohle-Erdgas-Petrochem 1989;42:294–7.
[40] Rodriquez NM. A review of catalytically grown carbon nanofibers. J Mater Res 1993;8:3233–50.
[41] Baker RTK. Carbon fibers, filaments and composites NATO ASI Series. Dordrecht: Kluwer; 1990, p. 405–39.
[42] Hammel E, Tang X, Trampert M, Schmitt T, Mauthner K, Eder A, et al. Carbon nanotube sheets for the use as artificial muscles. Carbon 2004;42:1153–8.
[43] Wang Y, Wei F, Luo G, Yu H, Gu G. The large-scale production of carbon nanotubes in a nano-agglomerate fluidized-bed reactor. Chem Phys Lett 2002;364:568–72.
[44] Toebes ML, Bitter JH, Van Dillen AJ, De Jong KP. Impact of the structure and reactivity of nickel particles on the catalytic growth of carbon nanofibers. Catal Today 2002;76:33–42.
[45] Ros TG. Ph.D. thesis, Utrecht University, Utrecht, The Netherlands, 2002.
[46] Rodriquez NM, Chambers A, Baker RTK. Catalytic engineering of carbon nanostructures. Langmuir 1995;11:3862–6.
[47] Colomer JF, Piedigrosso P, Willems I, Cournet C, Bernier P, Van Tendeloo G, et al. Purification and characterization by HREM of multi-wall nanotubes produced by catalytic process. J Chem Soc Faraday Trans 1998;94:3753–8.
[48] Chen P, Zhang HB, Lin GD, Hong Q, Tsai KR. Growth of carbon nanotubes by catalytic decomposition of CH_4 or CO on A Ni–MgO catalyst. Carbon 1997;35:1495–501.
[49] Boellaard E, De Bokx PK, Kock AJHM, Geus JW. The formation of filamentous carbon on iron and nickel catalysts: III. Morphology. J Catal 1985;96:481–90.
[50] Baker RTK, Kim MS, Chambers A, Park C, Rodriquez NM. The relationship between metal particle morphology and the structural characteristics of carbon deposits. Stud Surf Sci Catal 1997;111:99–109.
[51] Alstrup I. A new model explaining carbon filament growth on nickel, iron, and Ni–Cu alloy catalysts. J Catal 1988;109:241–51.
[52] Audier M, Oberlin A, Coulon M. Crystallographic orientations of catalytic particles in filamentous carbon; Case of simple conical particles. J Cryst Growth 1981;55:549–56.
[53] Schouten FC, Kaleveld EW, Bootsma GA. AES-LEED-ellipsometry study of the kinetics of the interaction of methane with Ni(1 1 0). Surf Sci 1977;63:460–74.
[54] Schouten FC, Gijzeman OLJ, Bootsma GA. Interaction of methane with Ni(1 1 1) and Ni(1 0 0); diffusion of carbon into nickel through the (1 0 0) surface; An AES-LEED study. Surf Sci 1979;87:1–12.
[55] Kim MS, Rodriquez NM, Baker RTK. Mat Res Soc Symp Proc 1995;368:99–104.
[56] Teunissen W. Ph.D. thesis, Utrecht University, Utrecht, The Netherlands, 2000.
[57] Kuvshinov GG, Mogilnykh YI, Kuvshinov DG, Yermakov DY, Yermakova MA, Salanov AN, et al. Mechanism of porous filamentous carbon granule formation on catalytic hydrocarbon decomposition. Carbon 1999;37:1239–46.
[58] Ledoux MJ, Pham-Huu C. Carbon nanostructures with macroscopic shaping for catalytic applications. Catal Today 2005;102:2–14.
[59] Vieira R, Ledoux MJ, Pham-Huu C. synthesis and characterization of carbon nanofibres with macroscopic shaping formed by catalytic decomposition of C_2H_6/H_2 over nickel catalyst. Appl Catal A 2004;274:1–8.
[60] Hadjiivanov K, Mihaylov M, Klissurski D, Stefanov P, Abadjieva N, Vassileva E, et al. Characterization of Ni/SiO_2 catalysts prepared by successive deposition and reduction of Ni^{2+} ions. J Catal 1999;185:314–23.
[61] Pina G, Louis C, Keane MA. Synthesis and characterization of carbon nanofibres with macroscopic shaping formed by catalytic decomposition of C_2H_6/H_2 over nickel catalyst. Phys Chem Chem Phys 2003;5:1924–31.
[62] Van Stiphout PCM, Stobbe DE, VDScheur FT, Geus JW. Activity and stability of nickel–copper/silica catalysts prepared by deposition–precipitation. App Catal 1988;40:219–46.
[63] Van Dillen AJ, Geus JW, Hermans LAM, Van der Meijden JJ. Production of supported copper and nickel catalysts by deposition–precipitation. In: Proc int congr catal 6th, vol. 2, 1976, p. 677–85.
[64] Winter F, Bezemer GL, Van der Spek C, Meeldijk JD, Van Dillen AJ, Geus JW, et al. TEM and XPS studies to reveal the presence of cobalt and palladium particles in the inner core of carbon nanofibers. Carbon 2005;43:327–32.
[65] Anderson PE, Rodriguez NM. Influence of the support on the structural characteristics of carbon nanofibers produced from the metal-catalyzed decomposition of ethylene. Chem Mater 2000;12:823–30.
[66] International patent number 04076211.4, Application date: 2004.
[67] Teunissen W, Hoogenraad MS. In: De Jong KP, Van Dillen AJ, editors. HeteroGEneoUS catalysis, preparation, characterization and application. Utrecht: Publicard; 1998. p. 137–55.
[68] Bitter JH, Van der Lee MK, Slotboom AGT, Van Dillen AJ, De Jong KP. Synthesis of highly loaded highly dispersed nickel on carbon nanofibers by homogeneous deposition–precipitation. Catal Lett 2003;89:139–42.
[69] Toebes ML, Van der Lee MK, Tang LM, Huis in 't Veld MH, Bitter JH, Van Dillen AJ, et al. Preparation of carbon nanofiber supported platinum and ruthenium catalysts: comparison of ion adsorption and homogeneous deposition precipitation. J Phys Chem B 2004;108:11611–9.